# Improved performance of Mn ion substituted Ceria nanospheres for low temperature CO oxidation and Water gas shift reaction: Influence of Calcination Temperature and Synthetic route

Thesis submitted to

Indian Institute Of Technology Hyderabad

in partial fulfillment of the requirements

for the award of the degree of

**M.Sc. in Chemistry**

**By,**

**SURAJIT SARKER**

(CY14MSCST11022)

Under the guidance of

**Dr. CH. SUBRAHMANYAM**

भारतीय प्रौद्योगिकी संस्थान हैदराबाद
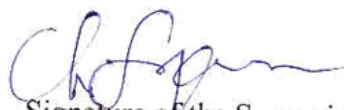**Indian Institute of Technology Hyderabad**

**DEPARTMENT OF CHEMISTRY**

**INDIAN INSTITUTE OF TECHNOLOGY**

**HYDERABAD-502285**

**APRIL 2016**

# Declaration

I hereby declare that the matter embodied in this report is the result of investigation carried out by me in the Department of Chemistry, Indian Institute of Technology Hyderabad under the supervision of **Dr. Ch. Subrahmanyam**.

In keeping with general practice of reporting scientific observations, due to acknowledgement has been made wherever the work described is based on the findings of other investigators.


Signature of the Supervisor


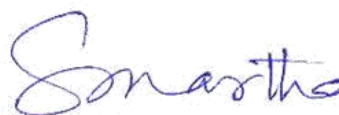*Swrajit Sarker*

(Signature)


*Swrajit Sarker*

(Student Name)


CY14MSCST11022

(Roll No)

# Approval Sheet

This thesis of the project entitled "**Improved Performance of Mn ion substituted Ceria nanospheres for low temperature CO oxidation and Water gas shift reaction: Influence of Calcination temperature and Synthetic route**" by **Surajit Sarker (CY14MSCST11022)** is approved for the award of the degree of **Master of Science** in Chemistry from **Indian Institute of Technology Hyderabad** during the year 2015-2016.

Dr. SURENDRA K. MARTHA
Assistant Professor      -Name and affiliation-
Department of Chemistry
Indian Institute of Technology Hyderabad

Examiner

-Name and affiliation-

Examiner

-Name and affiliation-

Adviser

-Name and affiliation-

Chairman

# ACKNOWLEDGEMENTS

Dedicated to

My mother, Late Sandhya Sarker, in her heavenly abode.

# Abstract

The catalytic activity described herein is aimed to portray various features associated with performance of manganese doped mesoporous ceria matrix. $Ce_{0.8}Mn_{0.2}O_{2-\Box\delta}$ is synthesized by facile co-precipitation, hydrothermal, combustion methods and calcined at $400^0C$, $600^0C$, $800^0C$. The activity tests demonstrate catalytic performance of $Ce_{0.8}Mn_{0.2}O_{2-\Box\delta}$ $400^0C$ is the best. The catalyst is characterized by physico-chemical techniques. XRD with Rietveld refinement points out decrease of crystallite size of manganese doped ceria. The absence of peak at $400^0C$ corresponding to dopant predicts generation of $Ce-Mn-O_x$ solid solution. BET-surface area measurement is employed to evaluate the structural properties like pore size, pore volume, surface area of the synthesized catalysts. SEM and TEM analysis determine spherical shape, state of aggregation, hexagonal surface morphology. UV-vis, Raman spectroscopic study are utilized to find oxygen vacancies. The present reporting minutely illustrates the outperforming aptitude $CM-400^0C$ among nine competitive catalysts.Their catalytic behavior towards CO oxidation is executed with 0.8 vol% CO with GHSV of 21,000 $h^{-1}$ as a model reaction with molecular oxygen as oxidant. The activation energy of low temperature CO oxidation with $CM-400^0C$ is found 5.49 kcal $K^{-1}mole^{-1}$. Water gas shift reaction is performed with $CM-400^0C$ prepared by co-precipitation method where $T_{50}$ is noted at $290^0C$.The higher activity of $Ce_{0.8}Mn_{0.2}O_{2-\delta}-400℃$ is supposed to be originated from the synergistic interaction of Mn(III)/Mn(II) and Ce(IV)/Ce(III) redox systems within $Ce-Mn-O_x$ solid solution. The catalyst is supposed to open a green method for saving environment from transcendental industrial progress.

# CONTENTS

# LIST OF ABBREVIATIONS

BET: Brunauer-Emmett-Teller

BJH: Barrett,Joyner and Halenda

CM-T: Cerium Manganese-Temperature

DRS: Diffuse Reflectance Spectroscopy

EDX: Energy Dispersive X-ray Spectroscopy

GHSV: Gas Hourly Space Velocity

HTS:  High Temperature Shift

IBT: Inter Band Transition

LTS: Low Temperature Shift

PEM: Proton Exchange Membrane

SAED: Selected Area Electron Diffraction

SEM: Scanning Electron Microscopy

TEM :Transmission Electron Microscopy

XRD: X-ray Diffraction

WGSR: Water Gas Shift Reaction

# Chapter 1

# Introduction

1.1: **Impact of Catalysis in greening environment.**

In this cutting edge of technological advancement, materialistic comforts control our necessities. The continuous development of industry and transport system though takes a giant step for mankind yet the progress put forwards severe adverse effects. Incomplete combustion of fuel in engines of cars, buses, trucks and other locomotives endangers our environment by emitting several greenhouse gases.The emission of oxides and hydrides of carbon, nitrogen, sulphur, halo alkanes, soot and other hazardous greenhouse gases from automobile industry gradually takes us on the verge of destruction. CO irreversibly binds with hemoglobin in a strong manner, thus appears fatal. The mutagenic and carcinogenic character of CO is an alarming phenomenon [2].In order to revive the environment from the tight grip of greenhouse gases stringent measures should be taken for CO oxidation, HC oxidation, and reduction of oxides of nitrogen. In atmosphere CO remains stable even at 700 °C for more than a week[3].The burgeoning challenge of decreasing carbon monoxide content of environment from alarming level to permissible level can be deal with transforming this to carbon dioxide[4].Until now, the prime resource of fuel of the contemporary world is fossil fuel. At present 75-85% of the world's energy demand are satisfied by fossil fuels. According to British Petroleum Company, the current fossil fuel reserve can run hardly 53.3 years provided the oil consumption rate remains same.[5]The energy content of the world is constant but usable form of energy continuously swings towards sustainable form.The depletion of diesel and gasoline turn the possibility of rolling the wheel of civilization at stake. In this burning context, an attempt to search an alternative chemical feedstock of energy reflects rationale of human being to surmount the fear of extinction. Hydrogen as a fuel is of high potential. 96% of the global hydrogen fuel is obtained from fossil fuels (high temperature steam reforming of natural gas yields 48%, refinery oil on oxidation gives 30% while 18% is obtained from coal gasification)[6]. Molecular Hydrogen has energy density by weight 141.80 MJ/Kg and for diesel it is 44.80 MJ/Kg[7].Molecular hydrogen is a potential clean and green fuel akin to PEM (proton-exchange membrane) fuel cell. Industries focused their attentions on applications of catalysis and targets to utilize thisin bringing down the cost of production, enhancing product quality and sustain green environment. The emphasis on developing catalytic converter using metal catalyst was one of the targeted fields of research during past few decades. Water gas shift reaction is a judicious selection of environmental chemists. Water gas shift reaction (WGSR)is one of the well-known heterogeneous reactions in industrial circuit (used in ammonia plant), now-a-days used for of clean energy technologies and renewable energy sources.The water gas shift (WGS) reaction is,   $CO + H_2O \leftrightarrows CO_2 + H_2$, $\Delta H_{298}^0 = -41.09$ kJ/mol

1

However depending upon the nature of catalysts and their optimum working temperature, two modes of WGSR are observed. High temperature shift (HTS) occurs at 350-800°Cusing Fe-Cr based catalyst.In-situ reduction of hematite ($Fe_2O_3$) produces magnetite ($Fe_3O_4$) which serves as an active sites of catalysts. In order to prohibit sintering action of $Fe_3O_4$,chromia ($Cr_2O_3$) is added as textural promoter. Chromium is an environmentally non friendly component.Spinel ferrite is thought to be an alternative[8]. Low temperature shift (LTS) occurs at 180-200°C using mixed oxide like $CuO-ZnO-Al_2O_3$ catalyst. These catalysts are pyrophoric.An efficient WGS catalyst must acquire, high thermal resistivity, non-pyrophoric nature, free from pre-activation arrangements, and redox active characteristics economically viable with high performance grade and must be robust during stringent start-up and shut down cycles. In order to address the problem getting an efficient nanocatalyst having profound catalytic activity towards oxidation of carbon monoxide is our prime target. In search of nano structured high performance grade heterogeneous catalyst, the solid solution of ceria and manganese oxide is extensively investigated.The present investigation is extended by covering water gas shift reaction under the preview of our work. Along with CO oxidation, by product hydrogen enhances the current reserve of this promising fuel. This treatise illustrates performance of nanostructured catalyst made by doping manganese oxide within ceria support (i.e. Mn ion substituted ceria) for low temperature CO oxidation and water gas shift reaction.

# LITERATURE SURVEY

**1.2: An Outline of Water Gas Shift Reaction (WGSR)**

In ammonia production plant (Haber's process) hydrogen is required as raw material. Industry attempted to get supply of hydrogen utilizing water gas shift reaction.The high temperature water gas shift reaction (HT-WGSR) involves Fe-Cr based catalyst was developed by Bosch and Wilde (1912). Hematite ($Fe_2O_3$) form is needed to be converted into catalytically active magnetite ($Fe_3O_4$) form. One familiar composition of high temperature catalyst has 74% $Fe_2O_3$ 10% $Cr_2O3$ and 0.2% MgO etc[9]. Addition of 2% (wt) of Pb, Ba, Cu, Ru, Ag and Hg enhances catalytic reactivity. Copper, silver, gold, ruthenium shows higher catalytic activity at HTWGS reaction. WGSR initiated methanation as parallel reaction, deactivating catalytic performance [10]. In order to prevent sintering action of iron oxide, chromia is used. CO concentration of the residual gas is measured less than 2% when the reaction is carried out at 673-773K.The low temperature water gas shift reaction (LT-WGSR) involves mixed oxide like $CuO-ZnO-Al_2O_3$ catalyst. Incorporation of redox active transition metal promotes WGS reaction. Incorporation copper lowers the operating temperature to 473 K – 573 K. Recently $CuFe_2O_4$ and $Al_2O_3$ composite is reported to carryout WGS in a significant fashion[11]. Low-Temperature Water Gas Shift (LT-WGS) reaction prefers copper since it lowers activation temperature to 453-473K. However copper is very sensitive towards sulphur. The catalyst loses its activity when sulphur content of raw materials remains high. Moreover low temperature catalysts are pyrophoric in character. [12]

### 1.3: Carbon monoxide, a tarnished gas.

Carbon monoxide (CO) is a colorless, odorless, apparently nonirritating gas. The abundance of CO in troposphere is below 0.001%. This concentration does not do any harm to mankind. Once its level crosses the borderline phase it poses a great threat. Carbon monoxide has a strong affinity towards haemoglobin and produces a kinetically stable carboxyhaemoglobin (COHb) thereby makes our body insufficient amount of haemoglobin to carry oxygen.This is all because of its extremely high bond energy -112.0933 a.u turns this as a stable molecule.The C-O bond length is 112.7 pm. This is a polar molecule having partial positive character on oxygen and negative charge on carbon. A Gaussian study is done with CO. Results are displayed in following scheme.

**Scheme 1: Different aspects of CO**
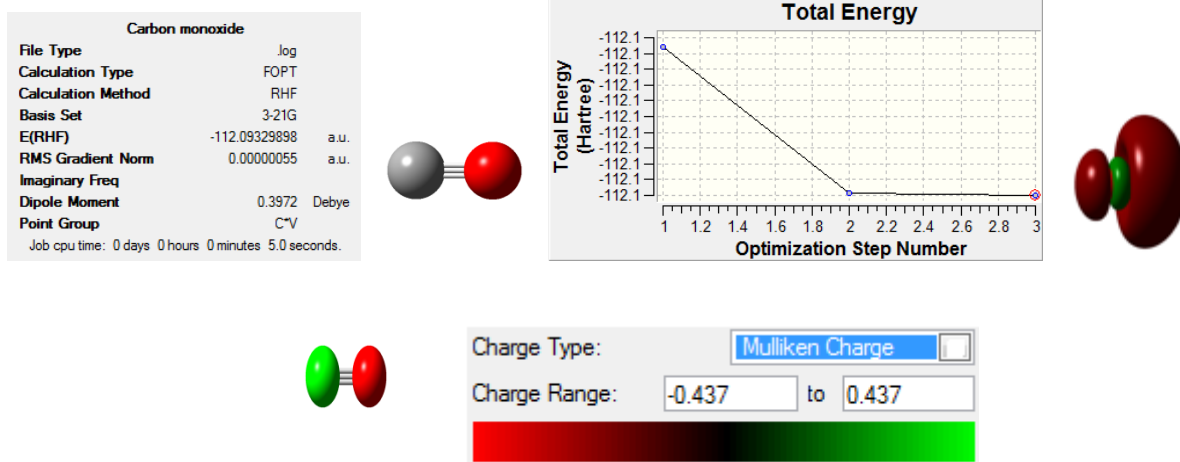


### 1.4: Ceria, a robust mesoporous support for nanocatalyst

Ceria exhibits its profound efficiency in water gas shift reaction, in solid-oxide based fuel cellsand in dehydrogenation reactions[13]. Cerium is about as abundant as copper. The ground state electronic configuration of $_{58}Ce$ is $[Xe]4f^15d^16s^2$.Thus Ce(IV) is most stable oxidation state and cerium dioxide, $CeO_2$ is a stable molecule. However 4f electron being in antepenultimate shell, is deeply shielded in comparison to penultimate and valence electrons. Thus Ce(III) is also appeared as predominant oxidation states.

Ceric and cerous couple formulates an effective redox couple.The crystal lattice of ceria has fluorite structure



where Ce is coordinated with eight oxygens and oxygen is tetrahedrally coordinated by cerium. Space group Fm3m (a = 0.541134nm, JCPDS 34-394)[14]. To visualize the structure, an fcc cube is considered where all corners are occupied by cerium ion and all tetrahedral holes are occupied with oxygen. Being smaller in size cerium cations cannot touched each other hence the structure is not a well packed structure. Octahedral holes in the crystal lattice are vacant.
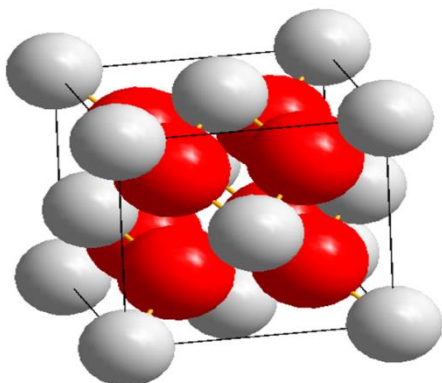
**Figure1: Fluorite structure of Ceria**

3

The exothermicity of WGSR is utilized by a ceria supported catalyst during dissociation of steam into hydrogen and oxygen. Ceria exhibits good oxygen storage capacity(OSC). The redox potential of Ce(IV)/Ce (III)couple is low. The origin of reactivity of ceria supported catalyst has been ascribed to this redox active aptitude of Ce(IV)/Ce (III). Simultaneous existence of many possibilities turns ceria as a redox active catalyst[15]. A number of cerium cation with various oxidation states appear resembling an automated engine with regular start up and shut down behavior. The preferred co-ordination number of Ce is eight. When Ceria is doped with other transition metals having lesser co-ordination number, a myriad of structural as well as electronic defects developed within ceria matrix. The perturbation turns ceria supported foreign metal composite a high performance heterogeneous nanocatalyst. Dopant in ceria, enhances Ce(III) content within the nano catalyst. The nimble catalytic activity of $Ce_{1-x}Mn_xO_{2-\delta}$ is observed owing to their high surface area to volume ratio. The high OSC of ceria is affected by sintering of ceria under reaction condition. Dopant reduces this tendency and keeps reducibility of ceria support intact. Metal modified cerium oxide thus has high oxygen storage capacity and reducibility then pure ceria. The oxide lattice supports fitting of transition metals inside the crystal structure, hence enhances its catalytic reactivity by many fold. The dopant produces a stress on the lattice structure. These defects develop many active sites on the catalyst surface. Moreover a number of very reactive oxygen entities like peroxide, oxides, monoxides are found in plenty inside nanocatalyst[13]. Noble metals like Pt, Pd, Ag, Au are easily doped within metal vacancy of ceria lattice. These composites are able to run the conversion at low temperature. Pt doped ceria catalyst is thoroughly investigated. A low temperatures CO oxidation is viable with Pt doped catalyst. Nobel metal based catalysts decreases operating temperatures. High expenditure, scarcity, sensitivity to CO or sulphur, deactivation at higher temperature directs to find out an efficient alternative. Nobel metals are also used with ceria-zirconia solid solution. The commercial catalyst preferred metal oxide doped catalyst though these performed the entire reaction at a slightly higher temperature.Recently incorporation of Ni, W within ceria lattice is reported. This initiates a synergistic interaction within Ni-W-Ce. Cu-based ceria, Ni-based ceria, Mn-based ceria are well known for catalytic activity[15]. Some well recognized catalysts are $Ce_{1-x}M_xO_{2-\delta}$ where M = La, Ti, Zr. Like Ceria, Titanium oxide, Copper-Ceria is found to more effective combination that other mesoporous copper based catalysts. Zr(IV) also forms a stable catalyst.[12].

**1.5: Manganese oxide as dopant**

The non-stoichiometric nature of $MnO_x$ assists this to supply oxygen during oxidation reaction[16]. The major advantages associated with manganese oxide are its compatibility with environment and of low economy. Apart from these, high specific capacitance makes it a combustion rugged material. The possibility of multiple oxidation states of manganese in its crystalline form is considered as the main source of its catalytic activity.

Moreover the morphology and crystalline character can be tuned by introducing shuttle changes during preparation of manganese oxide crystal.As a short profile of several activities of $MnO_x$, combustion of several organic compounds having volatile nature, dissociation of $NO_x$,ammonia oxidation are remarkable. Manganese oxide when doped in mesoporous ceria matrix, by co-precipitation method, dispersity of $MnO_x$ within ceria varies significantly. The orientation of Mn preferably directed towards surface hence catalyst appears more active. The coupling of two redox couples one based on cerium and other based on manganese produces a new redox system capable of exhibiting higher efficiency in CO-oxidation at low temperature.$MnO_x$-$CeO_2$ composite has higher degree of thermal stability. Recently combustion of chlorobenzene by this composite at 527K and oxidation of toluene at 523K are reported[13]. Low temperature (500K) combustion of chlorobenzene and toluene are also successful.[17]All these together make$Ce_{0.8}Mn_{0.2}O_{2-\delta}$ a promising catalyst for CO oxidation and Water Gas Shift reaction.

## 1.6: A Brief Timeline of last decade

**2001:**Hilaire et al. pointed the ceria supported transition metals used as catalysts for the water gas shift reaction.

**2003:**Apanee et al. noticed   $Pt/CeO_2$ is better than $Au/CeO_2$ and $Au/Fe_2O_3$.

**2004:** Wheeler et al.  introduced noble metals  with Ceria can run low temperature CO oxidation.

**2007:**Phatak et al.  usedPt supported on alumina and ceria at varying compositions for low temperature CO oxidation.

**2010:**Gonzaleza et al. found Pt catalysts supported on Titanium dioxide, ceria and cerium –Titania supports are compatible.

**2010:** Andrea et al.  usedPt, Rh, Pd and Au supported on Ceria.


## 1.7: Objectives of this Treatise.

The objectives of the present investigation are short-listed below.

➢ Synthesis of nano-architectured Mn ion substituted ceria catalysts.

➢ Characterization of the catalysts by various physicochemical methods.

➢ The activity of the catalyst is monitored by CO-$CO_2$–NO analyzer by measuring percentage composition of carbon monoxide and its oxidized product in ppm level as a function of temperature.

➢ The catalytic activity of $Ce_{0.8}Mn_{0.2}O_{2-\delta}$400$^0$C to 800$^0$C towards water gas shift reaction is investigated and the percentage of CO oxidation is measured at low temperature.

# Chapter 2

# Experimental Section

## 2.1: Experimental

Concise descriptions of experimental procedures are documented in this chapter. Depending on the specific synthetic route, catalyst having minute difference in structure can be produced. The difference is reflected in diversity of catalytic properties. The catalyst preparation scheme is vital since the method directly controls surface area, pore size, grain boundary, nature of non stoichiometry, various types' lattice defects in the structures etc which are crucial for the activity of the catalyst. Doping with manganese metal within ceria lattice is varied in different methods of preparation in order to achieve catalytic material compatible with low temperature activation.

## 2.1.1: Synthesis of CM-400 °C in fluorite phase by co-precipitation method.

| Materials used |
|---|
| $(NH_4)_2Ce(NO_3)_6$ (Merck, AR grade) |
| $Mn(NO_3)_2 \cdot 4H_2O$ (Sigma Aldrich, AR grade) |

**Scheme2: Shorthand representation of CM-400°C preparation by co-precipitation method.**
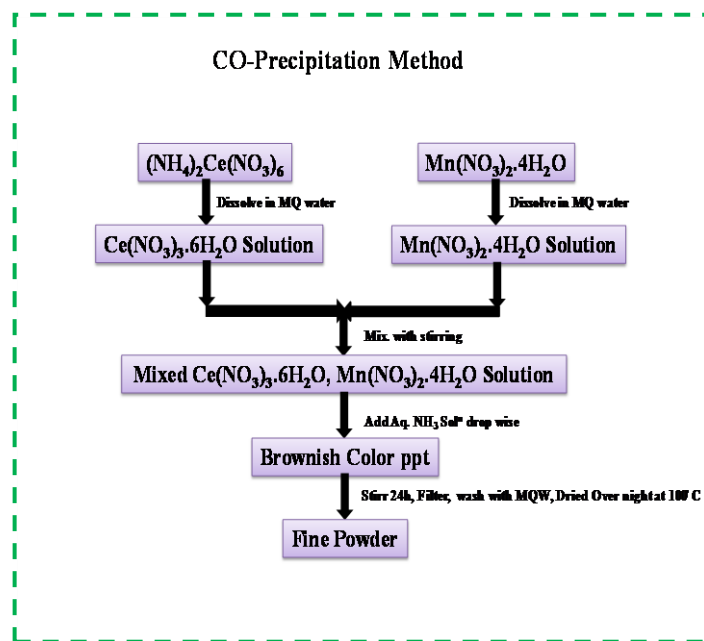


In a typical synthesis, 8mmol ceric ammonium nitrate (4.38g) is dissolved in sufficient amount of Milli Q water, 2mmol hydrated manganese nitrate (0.5g) is alsodissolved in sufficient amount of Milli Q water. Two solutions are made extremely dilute by adding Milli Q water. Two solutions are mixed with mild stirring condition. Dilute aqueous ammonia is added dropwise into the mixture and vigorously stirred. At pH = ~9.5, a brownish colour precipitate is found. The precipitate was continuously stirred for 24 h.This is kept overnight. The brown precipitate is filtered, washed with double distilled water to eliminate nitrate and alkali from residual solution.

6

The brown precipitate is oven dried overnight at 100℃. The dried precipitate is crushed into fine powder with a ceramic mortar. To decompose the residual nitrates, finely dispersed powder is then calcined for 1 hr in a closed electric furnace at 400℃.

**Scheme 3: Cubic Fluorite structure of ceria& $Ce_{0.8}Mn_{0.2}O_{2-\delta}$**



**Ceria   (Ce:gray; O:red)**          **$Ce_{0.8}Mn_{0.2}O_{2-\delta}$ (Mn:violet)**
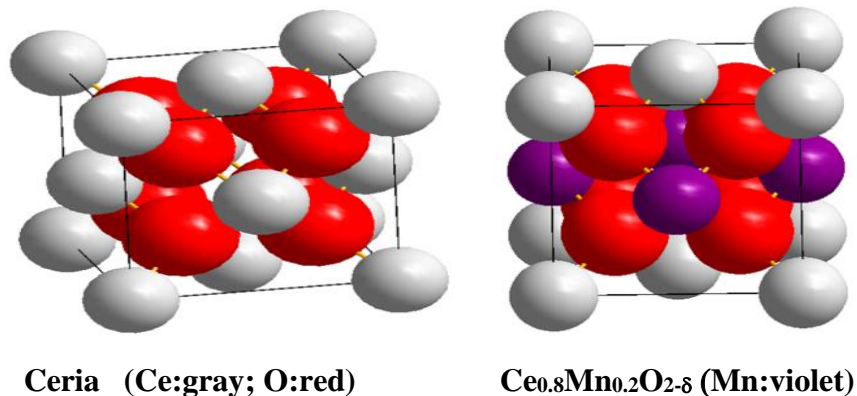
### 2.1.2: Synthesis of $Ce_{0.8}Mn_{0.2}O_{2-\delta}$ by combustion method.

Solution combustion (SC) is a traditional effective method for synthesis of nano-size materials. Nano crystalline materials are prepared through this method use an oxidizer and a fuel. Urea, hexamine etc are efficient fuels to synthesize the nanoscale materials.[19]



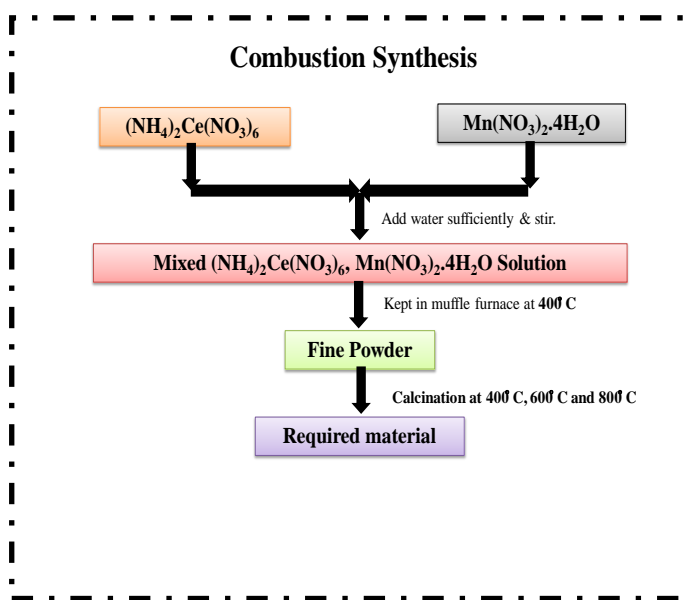In combustion synthesis of $Ce_{0.8}Mn_{0.2}O_{2-\delta}$, 8mmolceric ammonium nitrate (Merck; AR, 4.38g), 2mmol hydrated manganese nitrate (Sigma Aldrich;AR,0.5g) are taken in a beaker. The mixture is well dissolved in sufficient amount of MilliQ water.Then this solution was stirred at 300 rpm for few minutes. After that, the fuel, 35.3mmol urea (Fisher Scientific, AR 2.12g) is dissolved in minimum quantity of MilliQ water is mixed to the precursor nitrate solution and stirred well. Then, the solution combustion mixture was heated slowly in heating mantle until it gets ignited. This reaction mixture

is kept in a Muffle furnace at 400℃.The reaction mixture starts boiling with froth and foam. Sol-gel formation takes place. After complete dehydration, the residual mass is ignited (auto combustion) and a black solid is obtained. The solid is grinded to fine powder calcined at 400℃ for 1h. The black mass thus obtained is the targeted catalyst. $Ce_{0.8}Mn_{0.2}O_{2-\delta}$ is similarly calcined at600℃ and 800℃ and the thermal effect on the catalytic activity is investigated.

7

## 2.1.3: Synthesis of $Ce_{0.8}Mn_{0.2}O_{2-\delta}$ by Hydrothermal method.

| Materials required |
| :---: |
| $(NH_4)_2Ce(NO_3)_6$ (Merck, AR grade) |
| $Mn(NO_3)_2 \cdot 4H_2O$ (Sigma Aldrich, AR grade) |
| $CO(NH_2)_2$ (Fisher Scientific, AR grade) |

The chemical precursor's i.e 8mmol ceric ammonium nitrate (4.38g), 2mmol manganese nitrate tetrahydrate (0.5g) and 35.3mmol urea(2.12g) are well dissolved in double distilled water. The dissolved matter is now transferred into a Teflon vessel. 70% volume of the vessel is filled with water and the reaction set is kept in an autoclave. The solution is then pressurized well inside the reaction pot. The kettle is now kept in an oven at 120°C for 24 hrs. A solid crystallized out from the fluid. The solid is collected by filtration and grinded thoroughly to fine mesh and calcined the solid at 400°C for 1h. The fine solid is the targeted $Ce_{0.8}Mn_{0.2}O_{2-\delta}$.

# CHAPTER 3

# CHARACTERIZATION, RESULTS AND DISCUSSIONS

**3.1: Characterization of catalyst by XRD**

X-ray diffraction technique is a unique instrumental technique used for a number of qualitative as well as quantitative analysis of matter in solid phase. The analysis provides information about phase purity, transition between different phases of a substance, structure type, degree of crystallinity along with internal lattice strain, preferred crystal orientation, grain size, lattice parameters, average crystallite size.[20] The periodicity is the essence of crystallinity.

**3.1.1:X-ray diffraction data analysis**

Powder XRD patterns were carried out with prepared catalysts $Ce_{0.8}Mn_{0.2}O_{2-\delta}$ calcined at 400℃, 600℃ and 800℃ synthesized by combustion synthetic method. The diffractogram is compared with pure ceria and $MnO_x$ at 400℃. The diffractogram of ceria illustrates its existence in cubic fluorite phase with lattice parameter 5.4113Å(JCPDS No. – 34-0394).[22] The diffraction peaks showed in the diagram is assigned to (111), (200), (220), (311), (222), (400), (331), (420) lattice planes.
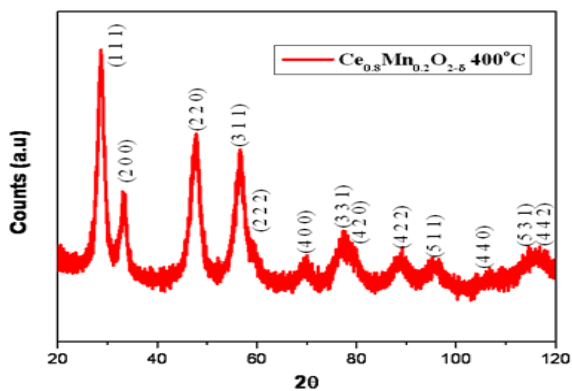


**Figure 2: Diffractogram of CM400℃**



**Figure3: Diffractogram of CM400°C, CM600°C, CM800°C.**
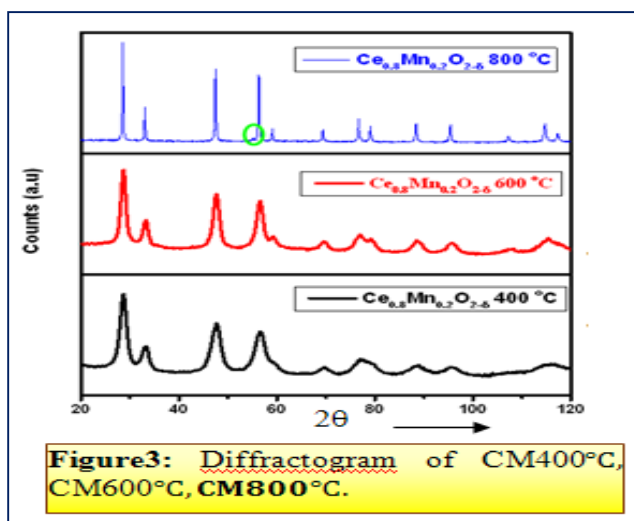
The diffraction peaks of CM 400℃, CM 600℃, CM 800℃, resemble with cubic fluorite phase akin to pure ceria. No diffraction peak corresponding to manganese oxide is noticed indicating formation of solid-solution. $Mn^{n+}$ is so well dispersed that it lost its individuality and the whole composite acquires higher degree of crystallinity. The sharpness of the peak notice is corroborated with crystallinity. $Mn^{n+}$ are smaller in size than Ce(IV). Ce(IV) is 0.097nm, $Mn^{2+}$ is 0.083 nm, $Mn^{3+}$ is 0.065 nm, $Mn^{4+}$ is 0.053 nm. Naturally replacement of Ce(IV) by $Mn^{n+}$ in ceria lattice hinders packing efficiency and induces lattice strain. But when calcination temperature increases from 400 ˚C to 800 ˚C the lattice parameter value is increased due to sintering of the material.

9

The lattice parameters calculated on the basis of major peak (111) planes of catalysts are tabulated in Table1.

**Table1: Crystallite size, lattice strain, Lattice parameter and cell volume from XRD**

| Catalysts | Crystallite Size (D in nm) | Lattice Strain (%) | Lattice parameter (Å) | Cell Volume (Å$^3$) |
|---|---|---|---|---|
| $CeO_2$ | 41.2 | 0.434 | 5.4137 | 158.66 |
| (400° C) $Ce_{0.8}Mn_{0.2}O_{2-\delta}$ | 8.9 | 1.664 | 5.3714 | 154.97 |
| (600° C) $Ce_{0.8}Mn_{0.2}O_{2-\delta}$ | 17.3 | 0.906 | 5.3828 | 155.964 |
| (800° C) $Ce_{0.8}Mn_{0.2}O_{2-\delta}$ | 58.6 | 0.328 | 5.4083 | 158.191 |

XRD calculation records lattice parameter for $CeO_2$ is highest and a gradual increase is noticed as one traverses CM 400℃ to CM 600℃to CM 800℃.This is supported by a slight increase of 2θ values of the diffraction peak. The lattice parameters of pure ceria and CM 800℃ are very close. This is an instance of phase separation of manganese oxide in ceria-manganese oxide solid solution. The appearance of an extra peak at 2θ for CM 800℃ at $55.22^0$ matched with characteristic peak of pristine $Mn_2O_3$ [11] (ICDD card No: 01 – 160). The smaller $Mn^{n+}$ when incorporated within ceria, triggers a lattice strain which ultimately resulted into Ce-Mn-$O_x$ solid solution. Moreover, the solid solution formation occurs at an ease at 400℃. Even at 600℃ solid solution occurs readily but at 800℃ it is somewhat doubtful about solid-solution formation. Below 800℃,well defind crystalline matters were formed. The crystallite sizes (D) of all catalysts were determined for $Ce_{0.8}Mn_{0.2}O_{2-\delta}$ using the most intense (111) peak using Scherrer equation. The peak shift towards higher 2θ value suggests a decrease of D. The XRD computation reveals D for pure ceria is 41.2 nm, D for CM400℃ is 8.9 nm, D for CM600℃ is 17.3 nm and D for CM 800℃ is 58.6 nm. The initial decrease of D suggests an inhibition of crystal growth.

The incorporation of $Mn^{n+}$ at lattice point targeted for Ce (IV) debars this natural growth of the crystal. The increase of calcination temperature has dual impact. The peaks appear more intense in association with decrease in peak width. This appearance is associated with high order of crystallinity. The increase of crystallite size (D)

is a reflection of periodicity of crystal growth. A dramatic change of D for CM800°C points out reduction of surface area. This may happen owing to segregation of $Mn^{n+}$ ion from Ce-Mn-O solid solution.



**Figure 4: Diffractogram of CM400°C**
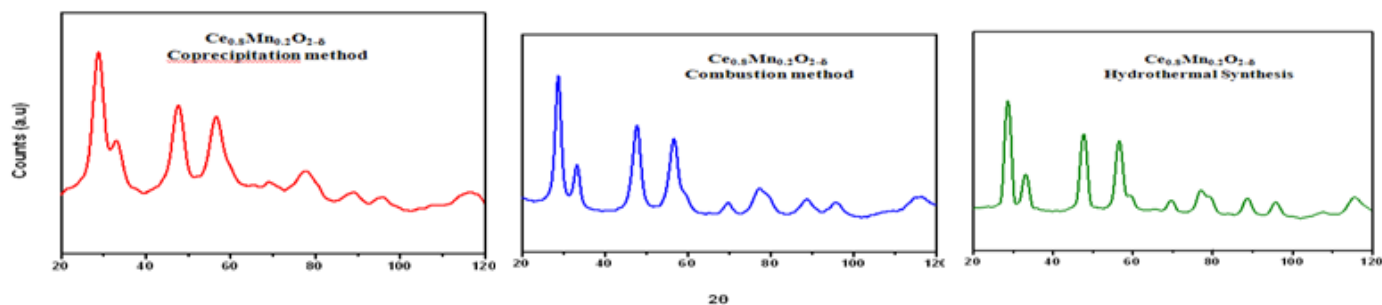
The Rietveld refinement analysis peak width showed a gradual decrease as calcinations of the catalyst are performed at higher temperatures. This illustrates the catalyst calcined at higher temperature is more crystalline. XRD data clearly describe increase of particle size (D) with the subsequent increase in calcination temperatures.
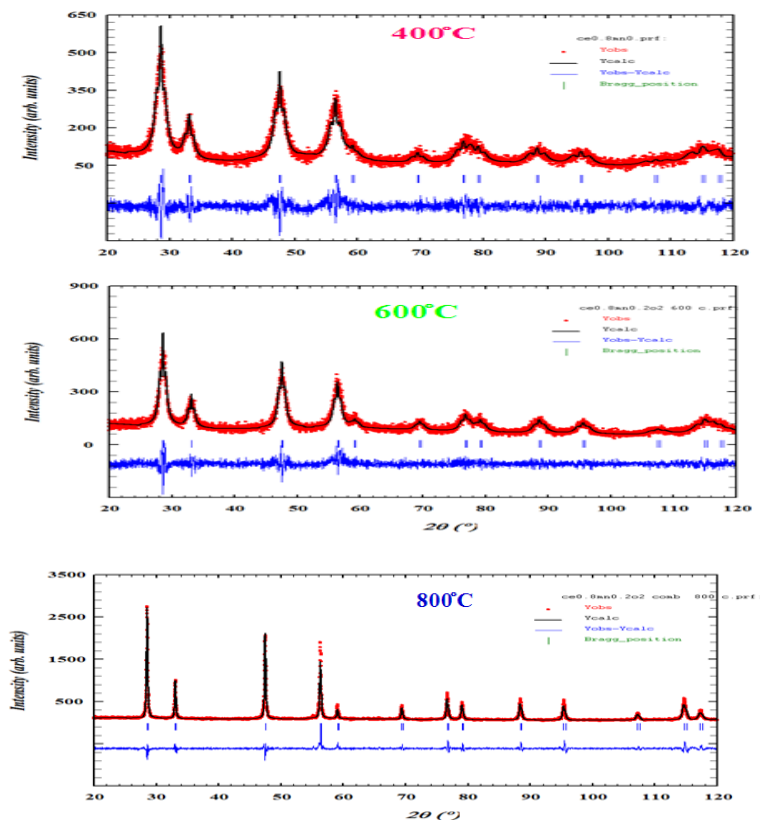


**Figure 5: Reitveld Refined XRD Spectra profile**

**Table.2: Cell Parameter, Cell Volume and Density from Reitveld Refinement data**

| Catalyst | Cell Parameter (A° ) | Cell Volume (cm$^3$) | Density g/cm$^3$ | $R_{bragg's}$ | $R_f$ | Chi$^2$ (c$^2$) |
|---|---|---|---|---|---|---|
| CeO$_2$ | 5.4117 | 158.49 | 7.364 | 7.64 | 3.43 | 4.60 |
| Ce$_{0.8}$Mn$_{0.2}$O$_{2-\delta}$ 400 C | 5.4041 | 157.82 | 7.771 | 4.44 | 2.65 | 2.00 |
| Ce$_{0.8}$Mn$_{0.2}$O$_{2-\delta}$ 600 C | 5.4064 | 158.03 | 7.338 | 5.66 | 3.14 | 1.77 |
| Ce$_{0.8}$Mn$_{0.2}$O$_{2-\delta}$ 800 C | 5.4145 | 158.73 | 8.078 | 7.41 | 3.73 | 2.53 |

In Table2, lattice parameters, cell volume, density, R-factors and reduced chi-square are tabulated. The lattice parameter also shows a gradual increase with calcinations temperature. Higher lattice parameters may arise from sintering of the calcined material.

**3.2: UV-VIS absorption Spectroscopy**

UV-Vis spectroscopy is used for characterization of nano catalysts. Emitted photon either has equal wavelength or longer wavelength since partial absorption is an unavoidable feature. Electronic transition from ground electronic state to excited electronic state requires a specific energy photon whose wavelength ranges from 200-750nm, hence the absorption spectrum is termed as UV-VIS spectra. The intensity of peak is related with higher molar extinction coefficient of absorbing materials. Absorption of UV-VIS photon promotes an electron from HOMO to LUMO. In case of charge transfer spectra, HOMO and LUMO belong to two different entities. Absorption of UV-VIS photon triggers various transitions. In pure ceria, HOMO of oxide ion and LUMO of cerium cation takes part in electronic transition. As manganese oxide is introduced as dopant, 3d orbitals appear LUMO in lieu of 4f orbital of Ce. The decrease of energy gap is reflected in absorption promoting a Red shift.

## 3.2.1: Diffuse Reflectance Spectroscopy (DRS)

Nanoarchitectured materials are characterized by this technique using Munk-Kubleka relation

$$\frac{k}{s} = \frac{(1 - R_\infty)^2}{2R_\infty}$$

In Shimadzu UV-vis spectrophotometer,taking $BaSO_4$ as internal standard,UV-VIS spectroscopy is performed in diffuse reflectance mode.

## 3.2.2: Analysis of UV–Vis, Diffuse-reflectance spectroscopy (DRS)



**Figure 6: UV–Vis spectrum of ceria**
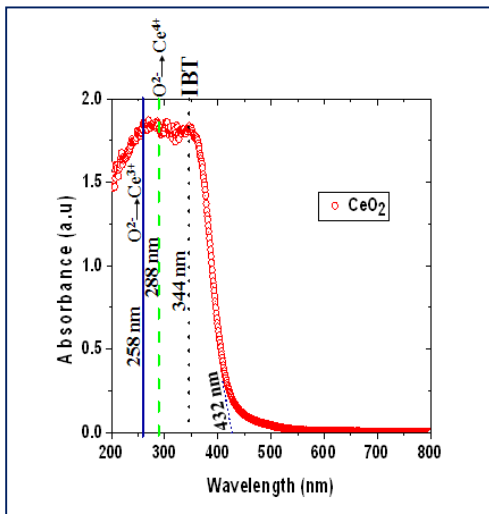
This technique provides information about d-d and d-f transitions taking place in a metal cation. An easy identification of ligand(oxide)-metal(Ce/Mn) charge transfer(LMCT) band  is possible in addition with determination of oxidation states of  metal within a solid solution.Figure6 represents UV–vis DRS spectra of pure ceria has three absorption maxima in UV region but no absorption is found in the visible zone. Peak at $\lambda$=258nm indicates $O^{2-} \rightarrow Ce^{3+}$ electronic transition, while peak at $\lambda$=288nm corresponds to $O^{2-} \rightarrow Ce^{4+}$ charge transfer transition and peak at $\lambda$=344nm illustrates inter band transition (IBT). DRS spectrum of $Ce_{0.8}Mn_{0.2}O_{2-\delta}$ at different temperatures is shown in Figure 7.



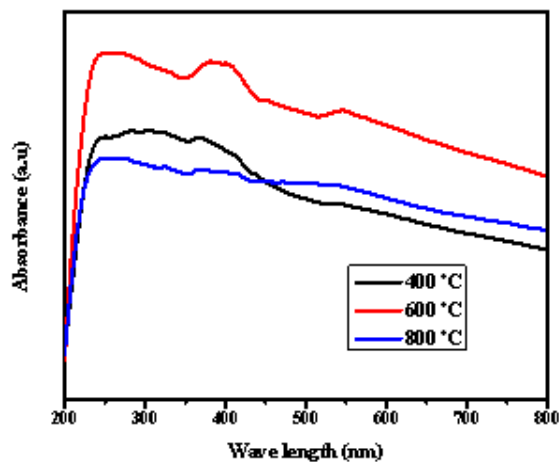**Figure 7:UV–Vis spectrum of $Ce_{0.8}Mn_{0.2}O_{2-\delta}$  at different temperatures.**

13

Intense absorption band at λ=245-255nm is originating from oxide to metal CT suggests incorporation of dopant which supplies lower energy LUMO. Thus a Red shift appears feasible. A peak at λ=385-410nm implies IBT. Doping with manganese oxide introduces several defects within the crystal thereby causing a red shift in absorption peaks. An extra peak in visible region of spectrum at λ=550nm appears. Mn can appear in various valence state and able to undergo several crystal field splitting generating many possibilities of electronic transitions. Dopant manganese offers 3d orbital as LUMO whereas LUMO of Ce is 4f. Obviously the electronic transition from HOMO of oxygen's 2p orbital to LUMO of Mn ion has higher molar absorbitivity since the transition is laporte allowed ($\Delta l = \pm 1$). The Red shift is connected with oxygen vacancy defects within ceria developed as a consequence of doping with manganese oxide. This directly augments catalytic activity of the $Ce_{0.8}Mn_{0.2}O_{2-\delta}$ solid solution. The absorption maxima at λ=525-550nm is recognized as forbidden d–d transition $^6A_1 \rightarrow {}^4T_1$ of $Mn^{2+}$. Thus doping of Mn within the $CeO_2$ lattice mostly occurs in Mn (II) state and a few Mn(III) is also found to be incorporated. UV–Vis spectrum of $Ce_{0.8}Mn_{0.2}O_{2-\delta}$ prepared by different methods is shown in Figure 8.
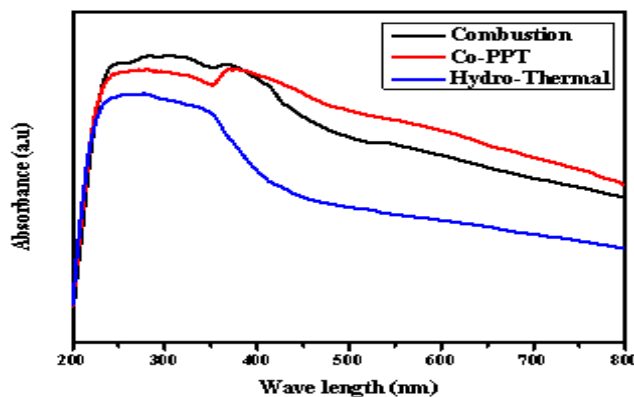


**Figure 8: UV–Vis spectrum of $Ce_{0.8}Mn_{0.2}O_{2-\delta}$ prepared by different methods.**

Among three absorption spectra, catalyst prepared by co-precipitation method shows strong absorption bands which points out myriad of oxygen vacancies within the catalyst playing a crucial function in CO-oxidation.

## 3.3: Raman Spectroscopy

In Raman spectroscopy change in polarization between two different states are essential. In present case, this investigation provides information about the presence of crystal defects arising by incorporation of manganese dopant in ceria lattice. Raman spectroscopic data are collected on a Bruker senterra dispersive micro Raman Spectrometer equipped with a confocal microscope and liquid nitrogen cooled charged detector by using a laser source of wavelength 532 nm.
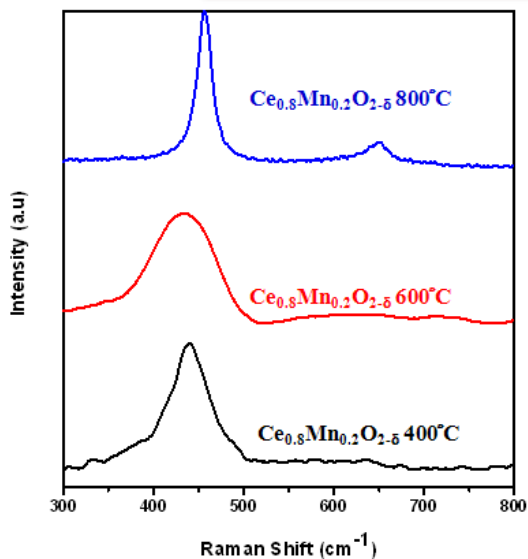
14

Figure 9: Vis-Raman spectrum of catalysts

The vis-Raman spectrum of $Ce_{0.8}Mn_{0.2}O_{2-\delta}$ at T = 400°C, 600°C, 800°C by combustion method are shown in Figure 9. A peak at~433cm$^{-1}$ is observed for $Ce_{0.8}Mn_{0.2}O_{2-\delta}$ prepared at 400°C by co-precipitation method while same catalyst shows Raman shift at 435 cm$^{-1}$ when synthesized by combustion and hydrothermal method (Figure 11). For $Ce_{0.8}Mn_{0.2}O_{2-\delta}$ prepared at 600°C a broadening of peak is noticed at 430cm$^{-1}$ however for $Ce_{0.8}Mn_{0.2}O_{2-\delta}$ calcined at 800°C the peak appears sharp but shifted towards 440cm$^{-1}$ along with an additional peak at 650cm$^{-1}$. Literature suggests a sharp peak at 460cm$^{-1}$ for pure ceria [16]. The peak is assigned to triply degenerate $F_{2g}$ active mode originating from vibration of the oxide species around ceric cations. The $F_{2g}$ active mode of all the CM samples calcined at different temperature is shifted to lower frequency, 430-440cm$^{-1}$.

For $Ce_{0.8}Mn_{0.2}O_{2-\delta}$ at 400°C, the highest shift suggests presence of more defect which increases oxygen storage capacity of the catalysts. A less prominent Raman shift is observed for $Ce_{0.8}Mn_{0.2}O_{2-\delta}$ at 800°C.The additional peak at 645-650cm$^{-1}$ is attributed to $Mn_2O_3$ indicating segregation of manganese oxide and ceria phase at higher temperature[11]. Oxide defect detected are prime source of catalytic activity.
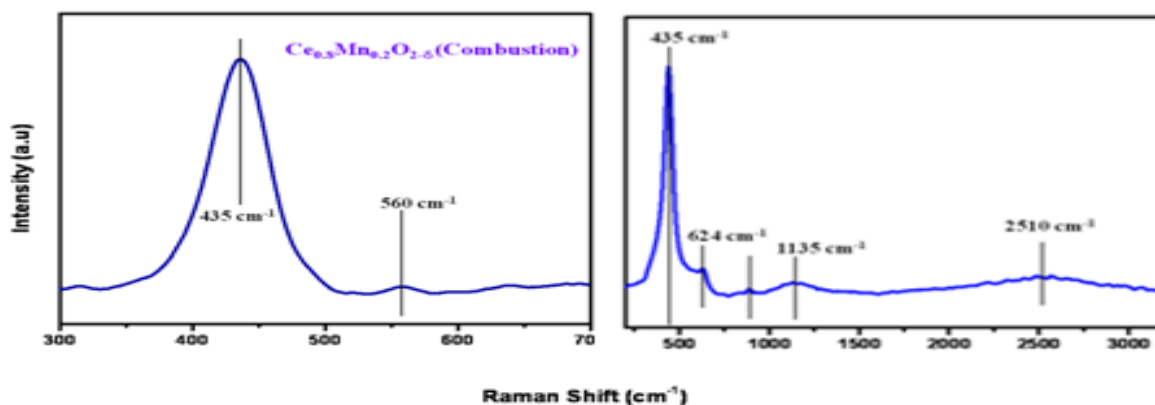


Figure 10: Vis-Raman spectrum of CM400°Csynthesized by Co-precipitation method



Figure 11: Vis-Raman spectrum of CM400°C synthesized by combustion and hydrothermal method

## 3.4: Determination of Surface area and porosity of catalysts.

The surface area (BET) and porosity of catalyst calcined at different temperatures are determined by nitrogen physisorption studies. The nitrogen adsorption–desorption isotherms Figure 12 and different surface characteristics like BET surface area, pore volume and pore diameter are tabulated in Table 3. The Barrett,Joyner and Halenda (BJH) method is employed for pore size and pore volume calculation. All samples are degassed at 573K for 3 hr in order to get rid off   already adsorbed impurities
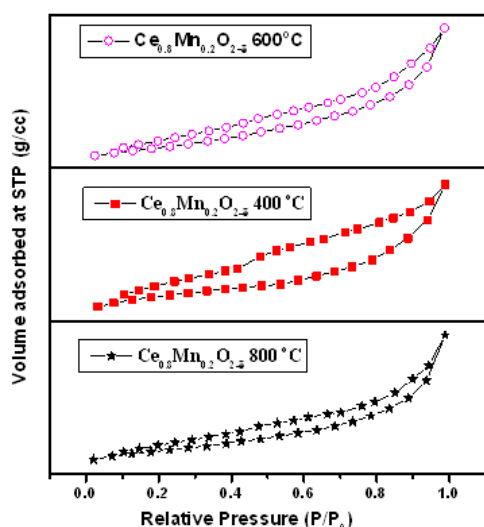


The results reveal that $Ce_{0.8}Mn_{0.2}O_{2-\delta}$ catalyst calcined at 400℃ by combustion method has the highest BET surface area 76 $m^2g^{-1}$and average pore size 13.18nm is highest among other catalysts calcined at 600℃ and 800℃. Pore size distribution on surface is crucial in making total surface area. All catalysts show adsorption-desorption isotherm in the relative pressure range of 0.8-0.97.

**Figure 12: Nitrogen adsorption-desorption isotherm**

**Table3: Surface characteristics of the $Ce_{0.8}Mn_{0.2}O_{2-\delta}$ catalyst prepared at different calcination temperature.**

| Sample | Surface area $(m^2g^{-1})$ | Average pore size (nm) | Total pore volume $(cm^3g^{-1})$ |
|---|---|---|---|
| $CeO_2$ | 31 | 14.03 | 0.0537 |
| $Ce_{0.8}Mn_{0.2}O_{2-\delta}$ at 400℃ | 76 | 13.18 | 0.1184 |
| $Ce_{0.8}Mn_{0.2}O_{2-\delta}$ at 600℃ | 55 | 4.35 | 0.1202 |
| $Ce_{0.8}Mn_{0.2}O_{2-\delta}$ at 800℃ | 44 | 5.11 | 0.1119 |

Distribution of Pore size as shown in Figure13 predicts mesoporous nature of catalysts.  Figure14 suggests catalyst calcined at 400℃ has highest surface area, hence exhibits highest catalytic activity. Keeping this fact under consideration, catalyst with same composition is prepared by co-precipitation and hydrothermal method. Investigation tabulated in Table3 reveals co-precipitation method produces catalyst with largest surface area, thus appears the best.
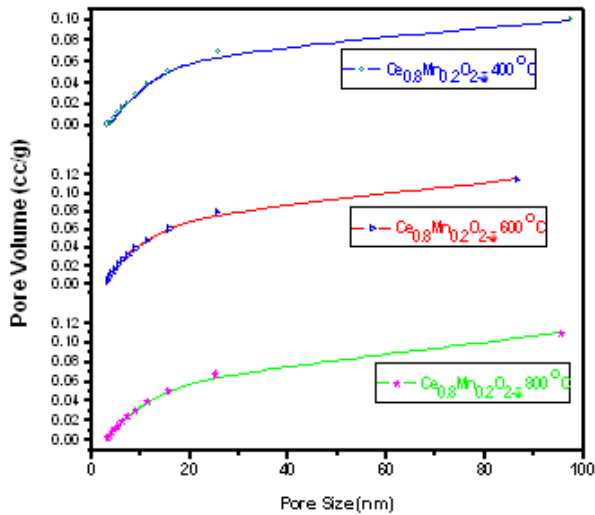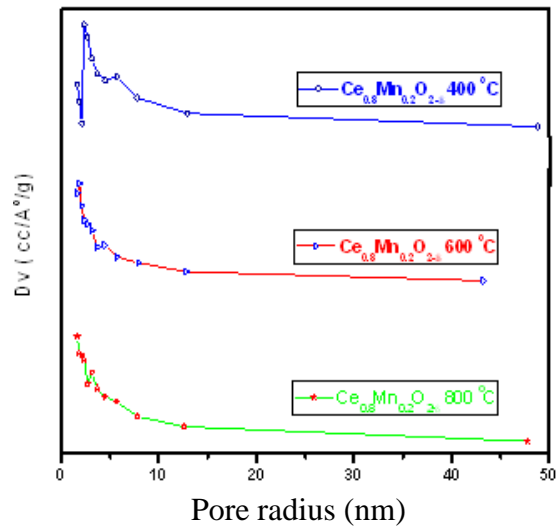
Figure13: Distribution of Pore size

Figure14: BJH Pore size distribution.

**Table3: Surface characteristics of the Ce$_{0.8}$Mn$_{0.2}$O$_{2-\delta}$ catalyst prepared by different methods.**

| Ce$_{0.8}$Mn$_{0.2}$O$_{2-\delta}$ at 400°C | Surface area (m$^2$g$^{-1}$) | Average pore size (nm) | Total pore volume (cm$^3$g$^{-1}$) |
|---|---|---|---|
| **Combustion** | 76 | 13.18 | 0.1184 |
| **Co-precipitation** | 126 | 5.43 | 0.3427 |
| **Hydrothermal** | 82 | 6.65 | 0.2744 |

When average grain size of nano particles decreases, surface area of certain amount of nanomaterials appears significantly high than particles with larger crystallite size (D).

## 3.5: Scanning Electron Microscopic (SEM) Study

Scanning Electron Microscopy (SEM) is a technique to study surface morphology of a solid matter.
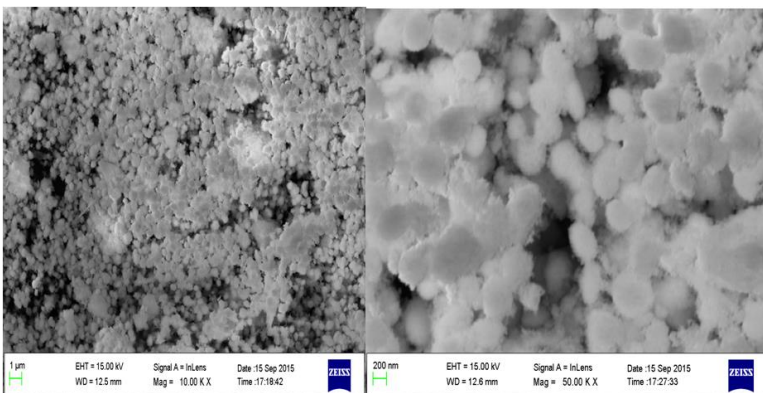


The micrographs for CM-400°C clearly illustrates that nanoparticles are well crystallized and are spherical in shape (Figure 15).The catalyst prepared via co-precipitation method appears well dispersed and appropriately distributed as compared to other competitive catalysts.

**Figure 15: SEM profile of Ce$_{0.8}$Mn$_{0.2}$O$_{2-\delta}$ method**

17
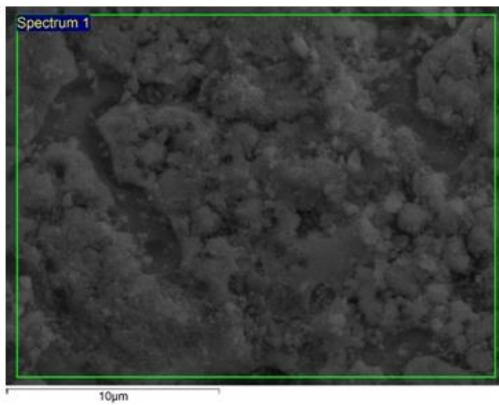
The SEM micrograph clarifies an agglomerated phase for catalyst prepared by combustion method (Figure 16). This reflects less crystallinity and lesser surface area. Agglomeration of nanoparticles often occurs since the nanoparticles tend to decrease the surface energy by decreasing the exposed surface area.

**Figure 16: SEM profile of $Ce_{0.8}Mn_{0.2}O_{2-\delta}$synthesized by combustion method**

The following elemental mapping (Figure 17) of $Ce_{0.8}Mn_{0.2}O_{2-\delta}$ confirms uniform distribution of Mn ions in the cubic fluorite phase of ceria.



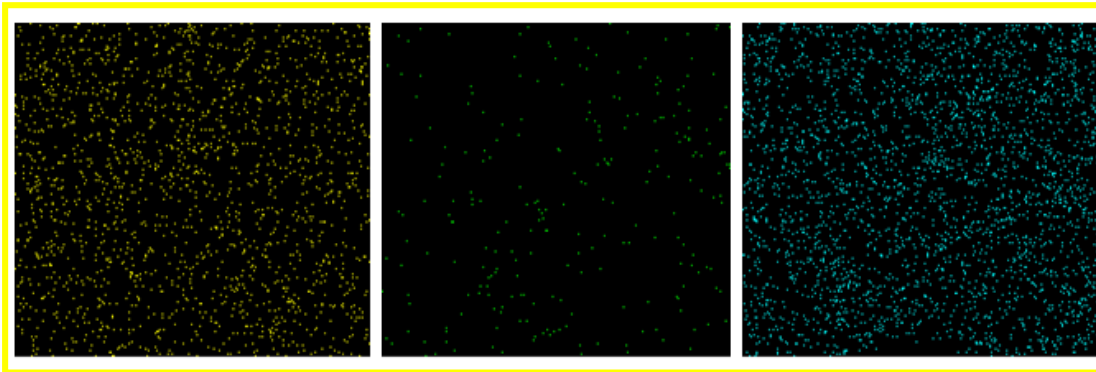Figure 17: Elemental mapping of $Ce_{0.8}Mn_{0.2}O_{2-\delta}$ (left for Ce, middle for Mn, right for oxygen)

The EDX investigation (Figure 18) displays peak corresponding to Ce and Mn. Moreover the Energy Dispersive X-ray Spectroscopic **(EDAX)** graph suggests 79.86% Ce and 20.14% Mn.
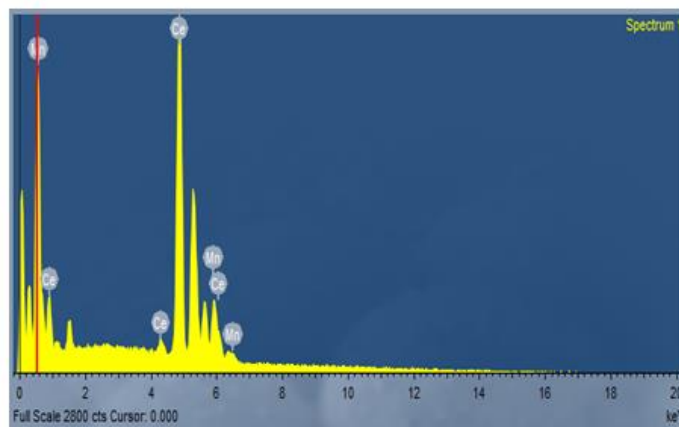


**Figure 18: EDX profile of $Ce_{0.8}Mn_{0.2}O_{2-\delta}$**

18

**3.6: Transmission Electron Microscopic (TEM) Study**

Transmission Electron Microscopy (TEM) is a microscopy based on diffraction characteristics of electrons.

The surface morphology of catalysts are investigated by TEM.TEM results suggest catalysts are monodispersed particles of size nearly 9nm.
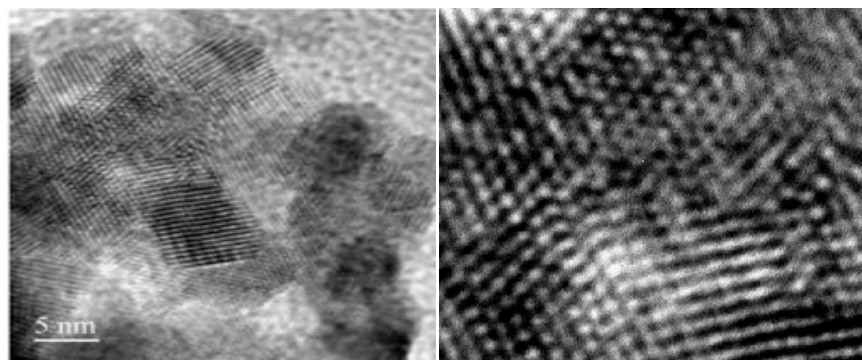
The HRTEM images (Figure19) illustrates one spherical size particle is closely surrounded by six similar sized spherical nanoparticles. In this way monodispersed layer acquires a hexagonal morphology. The HRTEM image (Figure20) exhibits well defined lattice fringes, illustrates crystalline nature of catalyst.



Figure20: The HRTEM image

The d-spacing of (111) lattice plane of $Ce_{0.8}Mn_{0.2}O_{2-\delta}$ prepared at 400℃ is observed **0.310** nm.In fluorite structure of ceria $d_{111}$ is found **0.309 nm**. Evidently no d-spacing corresponding to $MnO_x$ is noticed in HRTEM image. All these together suggest the dopant $MnO_x$ is well dispersed within cubic fluorite phase of ceria resulting into nanocatalysts. The selected area of micrograph has 318 particles and the corresponding particle size distribution is shown in Figure21.

From graph it is evident that the particle sizes fall within 8-9 nm. These selected area electron **diffraction** (SAED) of $Ce_{0.8}Mn_{0.2}O_{2-\delta}$ is consistent with the average crystallite size (D) 8.9nm as obtained from XRD measurements. The replacement of bigger sized cerium (IV) by smaller sized manganese cation in ceria lattice thus generates Ce-Mn-O solid solution. The diffraction image as shown in figure 22 illustrates Debye-Scherrer rings of the nanoparticles corresponding to cubic fluorite phase of $Ce_{0.8}Mn_{0.2}O_{2-\delta}$.
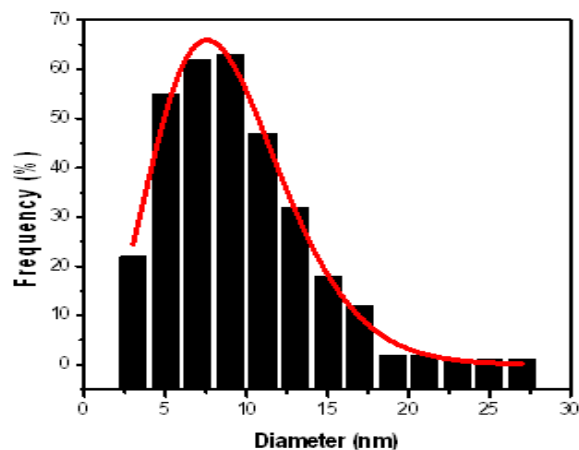
**Figure21: The particle size distribution**

The discrete ring renders crystalline feature of $Ce_{0.8}Mn_{0.2}O_{2-\delta}$ nano composite. The diffraction pattern of $Ce_{0.8}Mn_{0.2}O_{2-\delta}$ is compared with mesoporous ceria. No change in diffractograms demonstrates formation of Ce-Mn-O solid solution.
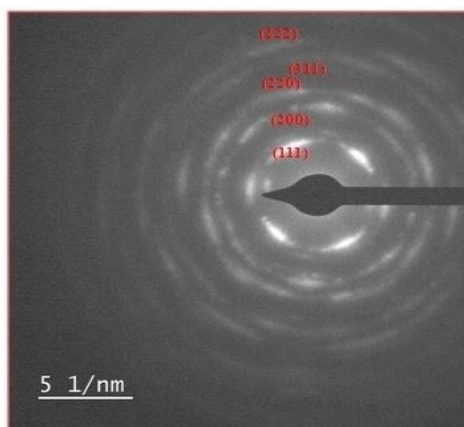

**Figure 22:Debye-Scherrer rings**

## 3.6.1:Computation of average particle size and polydispersity

Average nanoparticle size ($xc$) = 8.9683nm and **w** = 0.918nm.

Standard deviation ($\sigma$)=$\frac{w}{2}$ = 0.45905.

Thus average nanoparticle size (with error consideration) is $xc \pm \sigma$

$$= 8.9683 \pm 0.45905$$

$$= 8.50925 - 9.42735\text{nm.}$$

Polydispersity =$\frac{\sigma}{xc} \times 100\% = \frac{0.45905}{8.9683} \times 100\% = 5.12\%$

# CHAPTER 4
# ACTIVITY TEST ANALYSIS

## 4.1: ACTIVITY TEST

Nano composite matter $Ce_{0.8}Mn_{0.2}O_{2-\delta}$is now taken for analyzing its catalytic reactivity towards low temperature CO-oxidation and water gas shift reaction.The catalytic activity towards CO oxidation directly depends upon catalyst's surface area. The smaller particle size and defect oxygen species on the surface are likely to be the main source of catalytic activity. Smaller particle size has higher surface area. Several physicochemical techniques carried out earlier pointed out CM400℃ has least particle size hence large surface area. An increase in higher average grain size considerably decreases surface area. Crystallite growth occurs at higher calcination temperature,hence CM800℃ is expected to show lower reactivity. Moreover, segregation of $Mn_2O_3$ phase at higher temperature cuts off synergistic interaction between Ce and Mn based redox couple.

### 4.1.1: Source of Catalytic Activity

Langmuir-Hinshelwood proposed adsorbed CO on catalyst surface primarily get oxidized by adsorbed oxygen.[29] In this context reducibility of oxygen is very crucial. The defect oxygen species normally has a higher tendency for reduction. The catalytic activity depends upon surface active features like concentration of defect oxygen species on surface, the mobility of oxygen at the surface and within the bulk as well. The mobility of oxygen within the catalyst depends upon oxygen vacancies present in the composite. These oxygen vacancies are created within mesoporous ceria by Ce(IV)/Ce(III) couple's redox active behavior. Naturally this aptitude increases manifold when dopant manganese supplies another active Mn(III)/Mn(II) redox couple with the existing Ce(IV)/Ce(III). The synergistic interaction thus developes creates oxygen vacancies. Two redox active systems on coupling facilitates the generation of surface active oxygen vacancies. These vacancies on the surface in turn make easy accumulation of defect oxygen species at the surface at comparatively low temperature.

### 4.1.2: Plan of work

In the name of activity study, the present treatise targets to portray the optimization of non-noble metal based catalyst in greening environment. The entire scheme is divided into three stages. At first catalytic activity of $Ce_{0.8}Mn_{0.2}O_{2-\delta}$ calcined at different temperature is investigated. Among three catalysts CM400℃, CM600℃, CM800℃ , the best catalytic performance is noticed with CM400℃.

The temperature optimization is followed by optimization of synthetic methods. In this context, CM400℃ catalyst prepared by combustion, co-precipitation and hydrothermal method are taken for investigation. Treatment under identical condition reveals co-precipitation method sounds the best. The entire course of study is carried out for CO oxidation where molecular oxygen is the oxidizing agent. These oxidations occur easily in comparison to water gas shift reaction where steam is the source of oxygen. The endothermicity of water splitting demands higher energy. Prior to WGS reaction, the optimization scheme, running with CO-oxidation appears judicious. The following section would highlight how CM400℃ synthesized by co-precipitation method outperforms rest eight competitor catalysts.

## 4.2: Experimental Set up

Prior to investigation of catalytic activity, $Ce_{0.8}Mn_{0.2}O_{2-\delta}$ is heated in a fixed reactor at a rate of $10°C min^{-1}$. In a 200mm long quartz pipe of uniform diameter (6mm) weighted amount of catalyst (200/150/125/100/70/50mg) is taken. To keep catalyst fixed at its position two ends are fastened with ceramic wool.0.8% of CO balanced with dilutant nitrogen and 20% oxygen mixed again with nitrogen are passed in 1:1 ratio through the catalyst bed. CO flow rate is maintained at 150ml $min^{-1}$ while air is passed at a rate of 50ml $min^{-1}$. The flow rate of entire gas mixture is controlled at 200ml $min^{-1}$. Alaborg mass flow controller is used to achieve this. GHSV is maintained at $21000h^{-1}$. An infrared analyzer is connected with the experimental set up. This measures emitted CO, $CO_2$ after catalytic conversion.

## 4.3: Working formula for fractional CO conversion

The amount of CO conversion is calculated as, $CO^{\%}_{conversion} = \frac{[CO_{in}]-[CO_{out}]}{[CO_{in}]} \times 100$  …………(1)

$$[CO_{in}] \ is \ concentration \ of \ CO \ entered \ catalyst \ bed$$

$$[CO_{out}] \ is \ concentration \ of \ unreacted \ CO.$$

22

### 4.4.: Catalytic performance catalyst in light of CO oxidation

The catalytic performance of $Ce_{0.8}Mn_{0.2}O_{2-\delta}$ is portrayed in following sub categories.

### 4.4.1: Catalytic performance of CM400$^0$C, CM600$^0$C, CM800$^0$C

The catalytic activity of $Ce_{0.8}Mn_{0.2}O_{2-\delta}$ catalysts calcined at different temperature is tested for CO oxidation reaction and the results are displayed in Figure 23 The profiles for CO oxidation as a function of reaction temperature suggests calcination temperature is very important for performance of the catalyst. The comparison of the CO oxidation revealed that the catalytic activity of CM-400℃ outperforms rest catalysts as well as pure ceria in CO-oxidation.
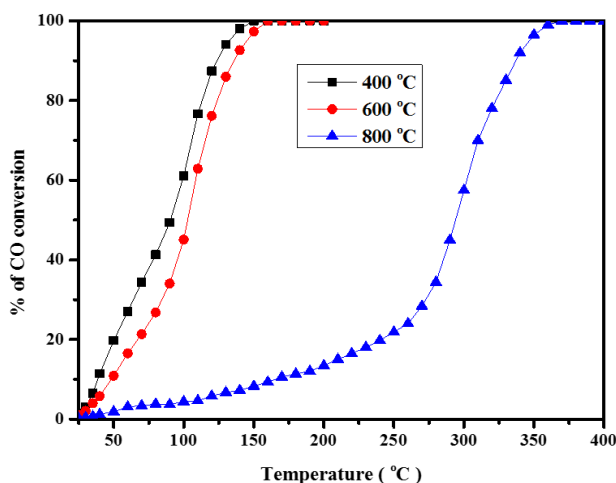


**Figure 23: Profile for conversion of CO (%) with reaction temperature using $Ce_{0.8}Mn_{0.2}O_{2-\delta}$catalysts calcined at different temperatures**.

CM-400℃ and CM-600℃ exhibit almost similar CO conversion upto150℃. However, catalyst calcined at 800℃ displayed substantially reduced activity than that of the catalysts prepared at 400℃ and 600℃. For CM-400℃ and CM-600℃, the light-off temperatures are observed at ∼90℃ and ∼105℃ respectively while CM-800℃ exhibits $T_{50}$ at ∼290℃. The investigation demonstrates that the optimum catalyst for low temperature CO oxidation is $Ce_{0.8}Mn_{0.2}O_{2-\delta}$ calcinated at 400℃ .

**4.4.2: Catalytic performance of CM400⁰C prepared by different synthetic methods**

After experimental detection of optimum calcination temperature, investigation is designed to carry out the experiment with $Ce_{0.8}Mn_{0.2}O_{2-\delta}$-400°C synthesized by different methods. The comparative catalytic activity is understood from the graphical view, Figure 24. Upto 60⁰C all exhibit similar activity but then onwards catalyst synthesized by co-precipitation method starts showing better activity. $T_{50}$ for which is noticed at ∼92 − 94°C. Catalyst produced by combustion and hydrothermal methods show similar catalytic behavior upto 90⁰C. Above this temperature hydrothermal method shows better activity. $T_{50}$ is observed at ∼102−103°C. $T_{50}$ for combustion method is found at ∼105°C.
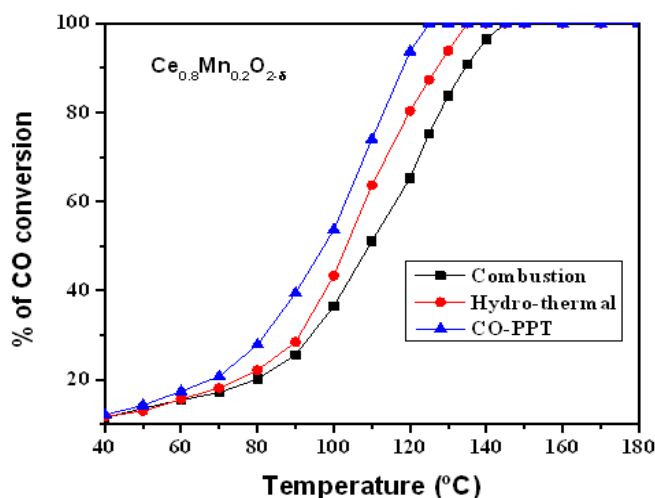


Figure 24: Catalytic activity of CM-400⁰C obtained by different methods

**4.4.3: Catalytic performance of CM400⁰C prepared by co-precipitation methods with varying amount of catalyst.**

Investigation is next designed to carry out the experiment with different amount of the $Ce_{0.8}Mn_{0.2}O_{2-\delta}$-400°C synthesized by co-precipitation methods. The CO oxidation is studied with varying amount of catalysts taking 50mg, 70mg, 100mg, 125mg, 150mg and 200mg in six separate experiments. Heterogeneous catalysis is primarily depends upon surface area. This is obvious that with large amount of catalyst at hand, more surface area is available. The catalytic activity with varying amount catalysts reaction temperature is shown in Figure25a & 25b.
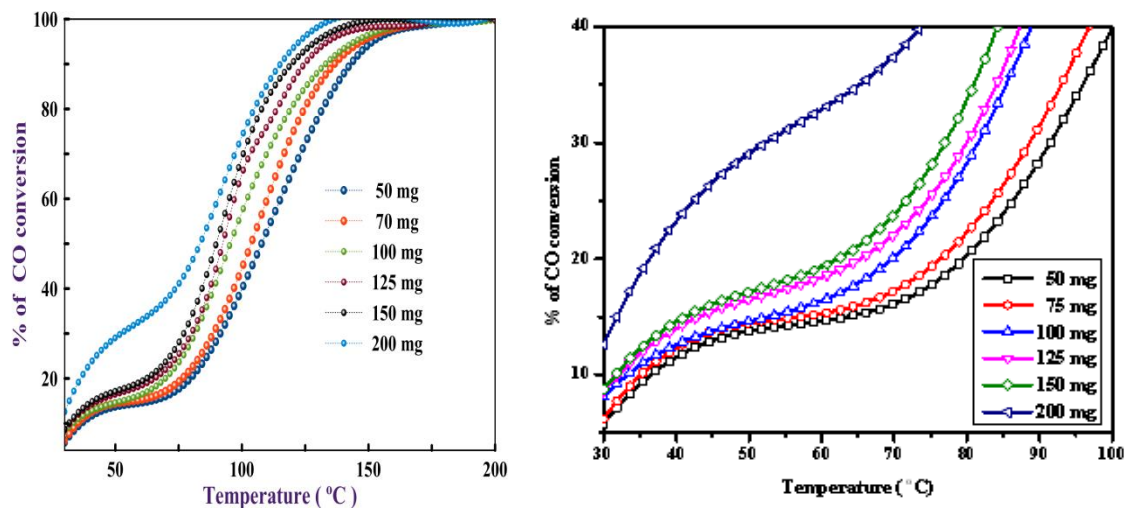
Figure25a & 25b: CO conversion with variable amount of starting $Ce_{0.8}Mn_{0.2}O_{2-\delta}$-400°C.

The comparative analysis reveals when starting catalyst is 200mg, the initial phase (upto 50% CO conversion) differs from the rest. $T_{50}$ is noticed at ~82-83°C. For rest catalysts upto 20% CO conversion all show same activity. Thus up to 60-63°C catalysts may not acquire proper activated phase and thus true colour of catalytic activity may not appear conspicuous. The comparative analysis reveals $T_{50}$~88 −92°C with 150mg, 125 mg and 100mg catalyst. $T_{50}$ for 70mg and 50mg appears at~104-108°C. The investigation thus demonstrates 200mg catalyst to be the best starting materials for achieving best results.

In next batch of experiment, 200mg catalyst is used for CO oxidation at different temperature ranging from $35^0C$ to $70^0C$ after every $5^0C$. The experimental findings are presented in Figure 26. Here x denotes fraction of conversion, w is the weight of catalyst, F is flow rate of CO and oxygen gas.
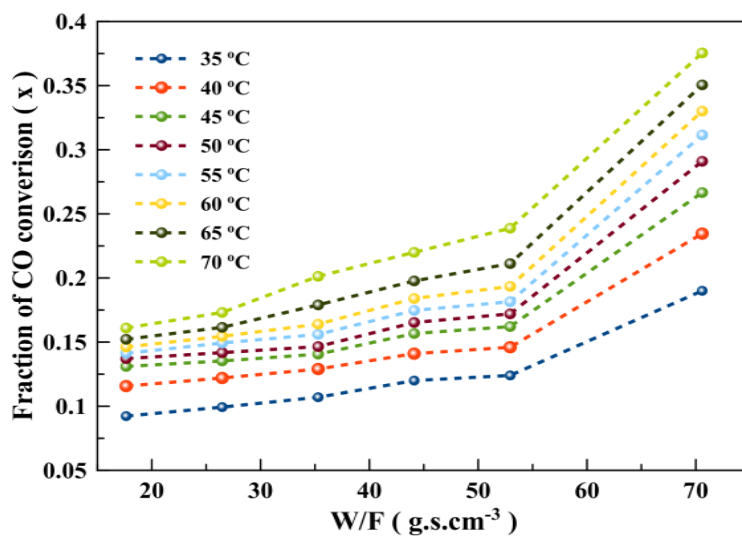


Figure 26: Fractional CO conversion Vs$\frac{W}{F}$ plot.

25

Fraction of CO conversion increases with temperature. Clearly slope graphical plot helps determination of rate of CO oxidation.x is calculated by equation(1).

$$Rate(r) = \frac{F}{W} \times x = \frac{x}{\frac{W}{F}} \ldots \ldots \ldots \ldots (2)$$

Rate of reaction at different temperatures are calculated using equation (2).

The linear relation of Rate ($\mu molg^{-1}s^{-1}$) Vs Temperature in $^0C$ plot is shown in Figure 27. The graph suggests CO oxidation rate is 0.009 $\mu molg^{-1}s^{-1}$ at $70^0C$.
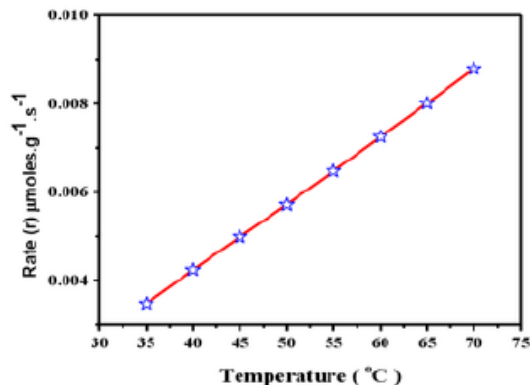


**Figure 27: Rate ($\mu molg^{-1}s^{-1}$) Vs Temperature in $^0C$ plot**

The energy of activation is calculated using Arrhenius equation (3).

$$k = Ae^{\frac{-E_a}{RT}} \Rightarrow lnk = lnA - \frac{E_a}{RT} \ldots \ldots \ldots \ldots (3)$$

$E_a$ is energy of activation, A is Arrhenius constant, R is Boltzmann constant, T is working temperature, k is rate constant. The $lnk$ vs $\frac{1000}{T}$ plot is displated by Figure 28. The slope of the curve denotes the energy of activation.
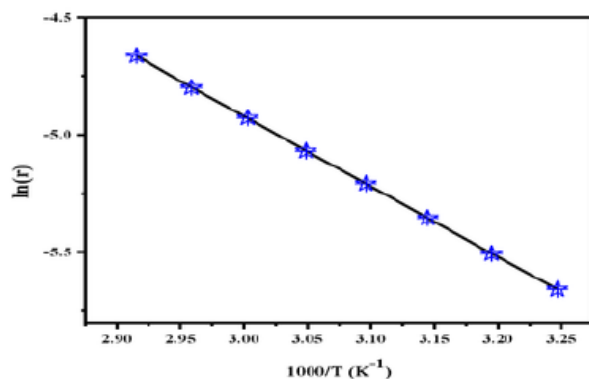


**Figure 28:** $lnk$vs$\frac{1000}{T}$ plot

The slope the linear plot is -2.763, energy of activation $E_a$ is calculated as 5.49 Kcal K$^{-1}$mol$^{-1}$.

26

## 4.5: Catalytic performance of CM400$^0$C prepared by co-precipitation methods in WGSR

The CO present in water gas is attempted to convert into carbondioxide by splitting steam into hydrogen and oxygen. Oxygen is spent for CO oxidation. In this activity test a hydrogen analyzer is attached to measure emitted hydrogen. The experimental set up is pictorially shown in Scheme 3.

### Scheme 4: Experimental set up for WGSR
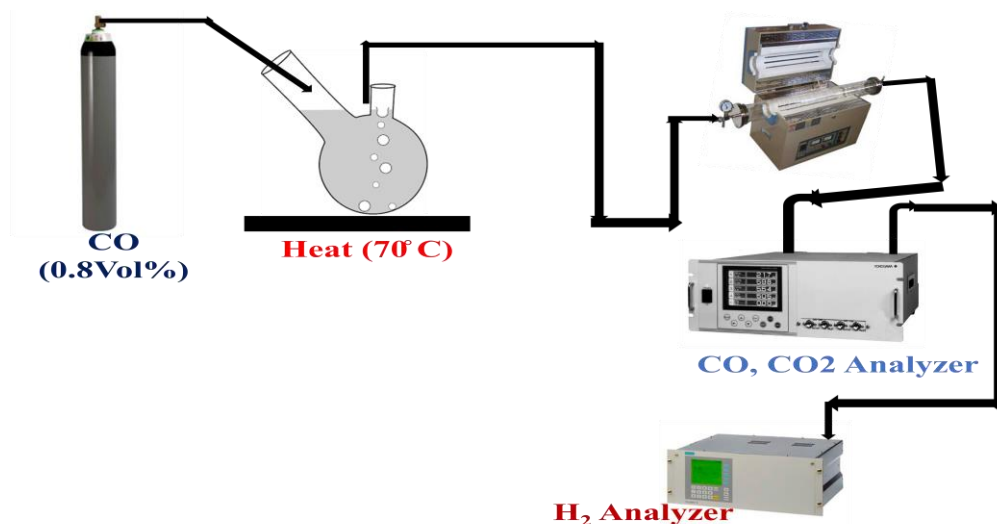


All relevant data concerning WGSR is tabulated in Table 4

### Table4: Experimental data of WGSR

| Name | Specification |
|---|---|
| $Ce_{0.8}Mn_{0.2}O_{2-d}$ | 400˚C |
| Amount of catalyst | 200 mg |
| Concentration of CO | 0.8 Vol% |
| Flow | 100 sccm (ml/min) |
| Temperature at water bubbler | 70˚ C |

The fractional CO conversion is displayed in Figure 29.
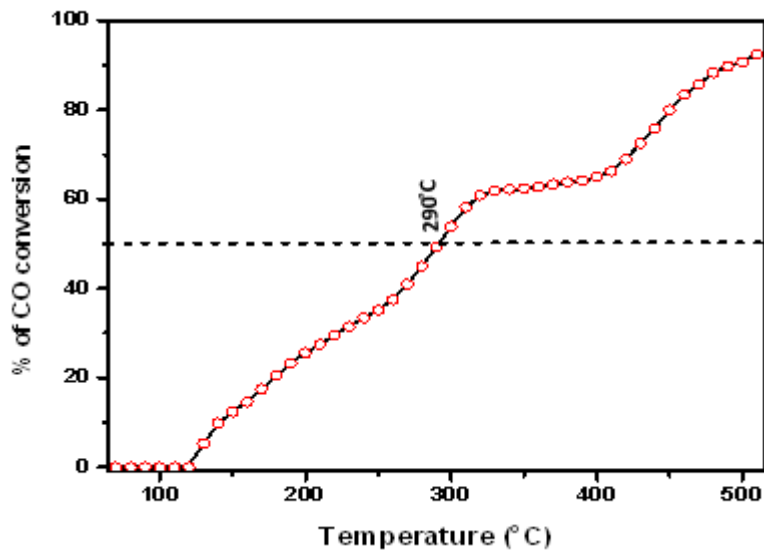


Figure 29: Fractional CO conversion as a function of temperature

This exemplify until $125^0C$, analyzer does not sense any amount of $CO_2$. Then onward CO oxidation begins. This might occur in order to overcome the endothermic characteristics of splitting of steam. From $125^0C$ to $325^0C$ range a regular CO oxidation is noticed in water gas. $T_{50}$ is found at $290^0C$. However from $325^0C$ to $450^0C$, a phase of catalytic innocence is observed. At this moment, the irregularity does not have a proper explanation. After 65% CO conversion, a little deactivation of active sites of catalyst takes place. $T_{98}$ is found at $500^0C$

# SUMMARY AND CONCLUSION

At the beginning of this chapter a brief summary of present investigation is illustrated.

**Chapter 1** gives the concise introduction regarding importance of catalysis in view of CO oxidation and water gas shift reaction, literature survey, characteristics of CO, ceria as catalyst, manganese oxide as dopant and objectives of the thesis.

**Chapter 2** describes the synthesis of manganese oxides doped ceria catalysts by co-precipitation, combustion, hydrothermal methods of which first method sounds best green method. Prepared catalysts are calcined at $400^0C, 600^0C, 800^0C$.

**Chapter 3** deals with characterization of the catalyst by a number of physicochemical techniques like XRD analysis, UV-Vis, Raman study, BET surface area measurement, SEM and TEM analysis.

XRD study points out drastic reduction of crystallite size in moving to $Ce_{0.8}Mn_{0.2}O_{2-\delta}$ -$400^0C$ from ceria.

UV-Vis study reveals doping with manganese oxide in ceria introduces several defects causing a red shift in absorption peaks.

Raman study exhibits nano composite materials mainly exist as solid solution. This also suggests segregation of $MnO_2$ phase at $800^0C$.

BET surface area study predicts highest surface area for $Ce_{0.8}Mn_{0.2}O_{2-\delta}$-$400^0C$.

SEM analysis suggests spherical shaped particles of $Ce_{0.8}Mn_{0.2}O_{2-\delta}$-$400^0C$ .

TEM study predicts hexagonal monodisperse phase and crystalline feature.

**Chapter 4** demonstrates catalytic activity of CM-$400^0C$ is unsurpassed with co-competitive catalysts.

In order to wrap up the investigation, the best catalytic performance by $Ce_{0.8}Mn_{0.2}O_{2-\delta}$-$400^0C$ synthesized by co-precipitation must be mentioned at the beginning. Co-precipitation method is a green method. The overwhelming CO oxidation noticed during activity test is attributed to surface area of $Ce_{0.8}Mn_{0.2}O_{2-\delta}$-$400°C 76 m^2 g^{-1}$ which is highest among three competitor catalysts. The mesoporoustexture of the ceria matrix assists catalyticbehaviour. The higher activity of $Ce_{0.8}Mn_{0.2}O_{2-\delta}$-$400°C$ is endorsed with high surface area, high OSC, high surface oxygen defects. This is assumed that defect oxygen species are prime species for oxidation. The incorporation of lower co-ordinated Mn ion in ceria lattice sets off a high strain inside the lattice.

This facilitates the mobility of oxygen ions through several channels created by oxygen vacancies. At the same time, this enhances the concentration of defect oxygen species at the surface. $MnO_x$ prevents the sintering of ceria crystallites. Incorporation of manganese causes strain inside the lattice, causing a decrease in the average crytallite size of the $Ce_{0.8}Mn_{0.2}O_{2-\delta}$. The success of WGS reaction at significantly low temperature ($T_{50}$~$290^0C$)

opens possibility of a new horizon to save the environment at a pace so as to match with the fast rolling wheels of industrial progress.

# References

[1] M.Newton, M. A., Dent, A. J., Diaz-Moreno, S., Fiddy, S. G., Jyoti, B., & Evans, J. (2006). Rapid Monitoring of the Nature and Interconversion of Supported Catalyst Phases and of Their Influence upon Performance: CO Oxidation to CO2 by γ-Al2O3 Supported Rh Catalysts. *Chemistry–A European Journal*, *12*(7), 1975-1985.

[2] Royer, S., & Duprez, D. (2011). Catalytic oxidation of carbon monoxide over transition metal oxides. *ChemCatChem*, *3*(1), 24-65.

[3] Salker, A. V., Choi, N. J., Kwak, J. H., Joo, B. S., & Lee, D. D. (2005). Thick films of In, Bi and Pd metal oxides impregnated in LaCoO 3 perovskite as carbon monoxide sensor. *Sensors and Actuators B: Chemical*, *106*(1), 461-467.

[4] Jha, A., Jeong, D. W., Jang, W. J., Lee, Y. L., &Roh, H. S. (2015). Hydrogen production from water–gas shift reaction over Ni–Cu–CeO 2 oxide catalyst: The effect of preparation methods. *international journal of hydrogen energy*, *40*(30), 9209-9216.

[5] Amadeo, N. E., &Laborde, M. A. (1995). Hydrogen production from the low-temperature water-gas shift reaction: kinetics and simulation of the industrial reactor. *International journal of hydrogen energy*, *20*(12), 949-956.

[6] Galletti, C., Specchia, S., Saracco, G., & Specchia, V. (2008). CO preferential oxidation in H 2-rich gas for fuel cell applications: microchannel reactor performance with Rh-based catalyst. *International Journal of Hydrogen Energy*, *33*(12), 3045-3048.

[7] Jeong, D. W., Jha, A., Jang, W. J., Han, W. B., & Roh, H. S. (2015). Performance of spinel ferrite catalysts integrated with mesoporous Al 2 O 3 in the high temperature water–gas shift reaction. *Chemical Engineering Journal*, *265*, 100-109.

[8] Smith, R. J., Loganathan, M., &Shantha, M. S. (2010). A review of the water gas shift reaction kinetics. *International Journal of Chemical Reactor Engineering*, *8*(1).

[9] Meshkani, F., &Rezaei, M. (2015). Preparation of nanocrystalline metal (Cr, Al, Mn, Ce, Ni, Co and Cu) modified ferrite catalysts for the high temperature water gas shift reaction. *Renewable Energy*, *74*, 588-598.

[10] Qi Fu, S. Kudriavtseva, H.Saltsburg, M. F.Stephanopoulos,Chem.Engineering Journal, 93 (2003) 41–53.

[11] Venkataswamy, P., Rao, K. N., Jampaiah, D., & Reddy, B. M. (2015). Nanostructured manganese doped ceria solid solutions for CO oxidation at lower temperatures. *Applied Catalysis B: Environmental*, *162*, 122-132.

[12] Dhannia, T. & Jayalekshmi, S. (2012). *Investigations on the structural, optical and Magnetic properties of nanostructured cerium oxide in pure and doped forms and its polymer nanocomposiets* (Doctoral dissertation, Cochin University of Science and Technology).

[13] Petallidou, K. C., Boghosian, S., &Efstathiou, A. M. (2015). Low-temperature water–gas shift on Pt/Ce 0.5 La 0.5 O 2− δ: Effect of support synthesis method. *Catalysis Today*, *242*, 153-167.

[14] Sunkari, S. (2011). Synthesis and structure of some coordination polymers of silver (i), cerium (iv) and manganese (iii).

[15] Meshkani, F., &Rezaei, M. (2014). A facile method for preparation of iron based catalysts for high temperature water gas shift reaction. *Journal of Industrial and Engineering Chemistry*, *20*(5), 3297-3302.

[16] Venkataswamy, P., Jampaiah, D., Rao, K. N., & Reddy, B. M. (2014). Nanostructured Ce 0.7 Mn 0.3 O 2− δ and Ce 0.7 Fe 0.3 O 2− δ solid solutions for diesel soot oxidation. *Applied Catalysis A: General*, *488*, 1-10.

[17] Dhannia, T., &Jayalekshmi, S. (2012). *Investigations on the structural, optical and Magnetic properties of nanostructured cerium oxide in pure and doped forms and its polymer nanocomposiets* (Doctoral dissertation, Cochin University of Science and Technology).

[18] Wu, X., Liu, S., Weng, D., Lin, F., & Ran, R. (2011). MnO x–$CeO_2$–$Al_2O_3$ mixed oxides for soot oxidation: Activity and thermal stability. *Journal of hazardous materials*, *187*(1), 283-290.

[19] Meshkani, F., &Rezaei, M. (2015). Preparation of nanocrystalline metal (Cr, Al, Mn, Ce, Ni, Co and Cu) modified ferrite catalysts for the high temperature water gas shift reaction. *Renewable Energy*, *74*, 588-598.

[20] Meshkani, F., &Rezaei, M. (2014). High temperature water gas shift reaction over promoted iron based catalysts prepared by pyrolysis method. *International Journal of Hydrogen Energy*, *39*(29), 16318-16328.

[21] Kunkalekar, R. K. (2013). Nanostructured based catalysts for detoxification of carbon monoxide gas.

[22] Xu, J., Deng, Y. Q., Luo, Y., Mao, W., Yang, X. J., & Han, Y. F. (2013). Operando Raman spectroscopy and kinetic study of low-temperature CO oxidation on an α-$Mn_2O_3$nanocatalyst. *Journal of Catalysis*, *300*, 225-234.